Fluorescent Probes

International Edition: DOI: 10.1002/anie.202001675
German Edition: DOI: 10.1002/ange.202001675

An Activatable AIEgen Probe for High-Fidelity Monitoring of Overexpressed Tumor Enzyme Activity and Its Application to Surgical Tumor Excision

Haidong Li[+], Qichao Yao[+], Feng Xu[+], Yueqing Li, Dayeh Kim, Jeewon Chung, Gain Baek, Xiaofeng Wu, Prima Fitria Hillman, Eun Young Lee, Haoying Ge, Jiangli Fan, Jingyun Wang, Sang-Jip Nam, Xiaojun Peng, and Juyoung Yoon**

Abstract: *Monitoring fluctuations in enzyme overexpression facilitates early tumor detection and excision. An AIEgen probe (DQM-ALP) for the imaging of alkaline phosphatase (ALP) activity was synthesized. The probe consists of a quinoline-malononitrile (QM) core decorated with hydrophilic phosphate groups as ALP-recognition units. The rapid liberation of DQM-OH aggregates in the presence of ALP resulted in aggregation-induced fluorescence. The up-regulation of ALP expression in tumor cells was imaged using DQM-ALP. The probe permeated into 3D cervical and liver tumor spheroids for imaging spatially heterogeneous ALP activity with high spatial resolution on a two-photon microscopy platform, providing the fluorescence-guided recognition of sub-millimeter tumorigenesis. DQM-ALP enabled differentiation between tumor and normal tissue ex vivo and in vivo, suggesting that the probe may serve as a powerful tool to assist surgeons during tumor resection.*

Introduction

The overexpression of enzymes in tumor cells, such as membrane type 1-matrix metalloproteinase (MT1-MMP),[1] aminopeptidase N (APN/CD13),[2] γ-glutamyltransferase (γ-GGT),[3] cyclooxygenase-2 (COX-2),[4] and alkaline phosphatase (ALP)[5] are important clinical indicators that are closely related to the occurrence, progression, and deterioration of tumors. The current consensus is that the early diagnosis and complete resection of cancerous tissue are particularly important in reducing cancer mortality, further relieving the heavy burden on families and society. The high selectivity, sensitivity, spatial resolution, and non-invasive characteristics of small-molecule fluorescent probes have made them indispensable for biological imaging.[6] There has been explosion in the development of fluorescent imaging agents associated with cancer diagnosis in recent decades, particularly for activatable fluorescent probes with high signal-to-noise ratios.[3e,7] These probes can help surgeons visualize tiny metastatic tumors to take preventive and therapeutic measures. Unfortunately, most traditional fluorescent probes suffer from the aggregation-caused quenching (ACQ) effect and readily leak out of cells during prolonged bio-imaging.[8] This limits the fidelity of long-term dynamic observations in biomedical and clinical research.

In 2001, Tang reported on the enhancement of fluorescence after molecular aggregation.[9] This phenomenon is referred to as aggregation-induced emission (AIE), which is directly opposite to the ACQ effect.[10] AIE has attracted a great deal of attention in the last decade[11] because fluorescent dyes that are capable of AIE do not have the inherent disadvantage of ACQ. AIE luminogens (AIEgens) generally have twisted propeller-shaped conformations or rotatable structures,[10b] which effectively restrict intramolecular motion and render intermolecular π–π interactions in the aggregation state to regulate the release of energy in the excited state, resulting in brighter fluorescence. This property makes AIEgens suitable for long-term, high-fidelity monitoring of target molecules in biological systems. Many researchers have focused on "always-on" AIEgens based on tetraphenylethylene (TPE) and hexaphenylsilole (HPS) fluorophore derivatives,[12] which are characterized by low signal-to-noise ratios. Photobleaching and photo-induced damage are less extensive in two-photon (TP) fluorescence microscopy.[13] TP fluorescence technology also provides higher 3D imaging resolution due to the nonlinear optical process at the most commonly used excitation wavelengths, which range from 700 to 1000 nm. Disappointingly, there are relatively few AIEgens for TP fluorescence microscopy, despite their superiority in biological imaging, to the best of our knowledge. 3D tumor

[*] Dr. H. Li,[+] D. Kim, J. Chung, G. Baek, Dr. X. Wu, P. F. Hillman, E. Y. Lee, Prof. Dr. S.-J. Nam, Prof. Dr. J. Yoon
Department of Chemistry and Nanoscience
Ewha Womans University, Seoul 03760 (Korea)
E-mail: jyoon@ewha.ac.kr
Q. Yao,[+] F. Xu,[+] H. Ge, Prof. Dr. J. Fan, Prof. Dr. X. Peng
State Key Laboratory of Fine Chemicals, Dalian University of Technology, 2 Linggong Road, Dalian 116024 (P. R. China)
E-mail: pengxj@dlut.edu.cn
Prof. Dr. Y. Li
School of Pharmaceutical Science and Technology, Dalian University of Technology, 2 Linggong Road, Dalian 116024 (P. R. China)
Prof. J. Wang
School of Life Science and Biotechnology, Dalian University of Technology, 2 Linggong Road, Dalian 116024 (P. R. China)
Prof. Dr. J. Fan, Prof. Dr. X. Peng
Research Institute of Dalian University of Technology in Shenzhen, Gaoxin South fourth Road, Shenzhen 518057 (P. R. China)
[+] These authors contributed equally to this work.
Supporting information and the ORCID identification number(s) for the author(s) of this article can be found under: https://doi.org/10.1002/anie.202001675.

These are not the final page numbers!

spheroids, which are spherical aggregates of tumor cells, bridge the distance between traditional 2D cell culture models and complex real tissues.[14] Moreover, they can provide more realistic and economical research models for clinical and biological applications. In current research models, the difference in scale between living cells and the in vivo level may lead to an incomplete understanding of tumor onset, progression, and deterioration mechanisms. Models at the sub-millimeter scale are lacking. In addition, few activatable AIEgens that can differentiate between cancer tissue from normal tissue to facilitate tumor resection have been reported. These gaps motivated us to develop an activatable two-photon AIEgen probe that would enable fluctuations in tumor enzyme overexpression to be detected and guide tumor surgery in clinical settings.

The quinoline-malononitrile (QM) chromophore has recently emerged as a new AIE building block.[15] It has the characteristics of controllable excitation/emission wavelength, facile modification, and good biocompatibility.[12] QM may be an alternative platform for the development of activatable AIEgens. Alkaline phosphatase (ALP; EC 3.1.3.1) is an enzyme containing one magnesium atom, two zinc atoms, and five cysteine residues.[16] In clinical practice, ALP is recognized as a critical biomarker associated with signal transduction and tumors metabolism.[17] Inspired by the target-response strategy, we selected the hydrophobic QM derivatives as the AIE core and hydrophilic phosphate group as the ALP-recognition unit to design the activated nanoAIEgen DQM-ALP (Scheme 1) for tumor diagnosis. The matched amphiphilic structure DQM-ALP enabled it to self-assemble into a loosely packed nanoprobe in aqueous solution. DQM-ALP molecules showed severe fluorescence quenching in vitro. Activation of the probe by ALP, induced the in situ aggregation of DQM-OH, which restricted free molecular rotation and restored its intrinsic AIE fluorescence. When cancer cells were incubated with DQM-ALP, overexpressed ALP in the cells cleaved its ALP-sensitive moieties. Stronger AIE fluorescence enabled high-fidelity tracking of fluctuations in ALP activity. DQM-ALP was rapidly delivered into 3D tumor spheroids and enabled the observation of ALP activity in the sub-millimeter multicellular aggregates. The DQM-ALP nanoprobe was successfully employed to distinguish normal tissue from cancerous tissue with high a signal-to-noise ratio, implying that DQM-ALP AIEgen has the potential to assist surgeons in removing tumors during surgery.

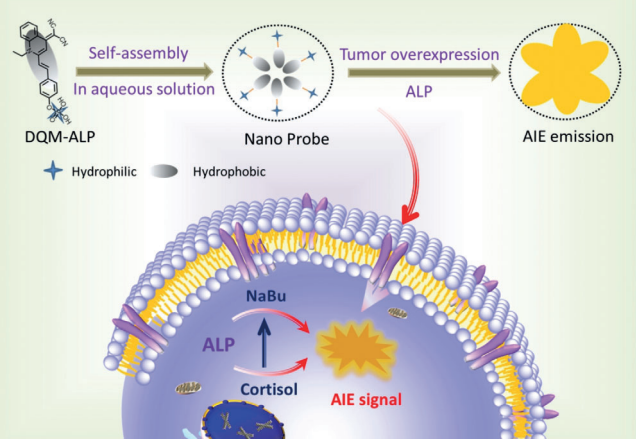

Scheme 1. Schematic illustration of the assembly of DQM-ALP and process of AIE activation in vitro and in cell.

Results and Discussion

Synthesis and Spectroscopic Characteristics

The intermediates, DQM-ALP, and DCM-ALP (contrast agent) were synthesized as shown in Scheme S2. Their full characterization by ^{1}H, ^{13}C, and ^{31}P NMR spectroscopy and HRMS is described in the Supporting Information (Figures S1–S27). To validate the initial design concept, DQM-ALP nanoaggregates were obtained by dispersing a DQM-ALP stock solution in DMSO into the aqueous solution. Nanoaggregates of the amphiphilic structure were confirmed by dynamic light scattering analysis (DLS, Figure 1a) and TEM (Figure 1b).

The effect of the volume fraction (f_w) of distilled water (DW) on UV/Vis absorption and fluorescence of DCM-OH, DCM-ALP, DQM-OH, and DQM-ALP was evaluated using DW/DMSO mixtures. As displayed in Figures S28–S30, the DQM-ALP spectra were almost unaffected by increases the f_w, which were accompanied by low quantum yields (Φ) ranging 0.4% to 0.1%. Fluorescence images of DQM-ALP solutions confirmed that no AIE occurred (Figure S31). The DCM-ALP exhibited similar spectral behavior (Figure S32–S34). However, when the ratio of DW in the mixed solvent exceeded 70%, the fluorescence intensity of DQM-OH increased sharply due to restricted rotation of the *N*-ethyl group (Figures S35 and S36). The quantum yield increased 13-fold, which was indicative of AIE (Figure S37). The absorption spectra of DQM-OH decreased markedly with increasing f_w, which was due to the scattering effect of DQM-OH aggregates (Figure S38). The DLS and TEM data confirmed the presence of DQM-OH aggregates in aqueous solution (Figures S39 and S40). In contrast, the ACQ behavior of compound DCM-OH was observed in the DW/DMSO mixtures, as shown in Figures S41–S43. As the pH value decreased (10.01–4.73), the fluorescence intensity of DQM-OH increased obviously (Figures S44 and S45). However, the weak ionization ability ($pK_a = 8.75$, Figures S46 and S47) of DCM-OH phenolic hydroxy group significantly restricted DCM-ALP for the detection of ALP in vitro (Figures S48 and S49). Subsequently, the excitation and emission spectra of DQM-ALP in the presence of ALP were investigated to determine the optimal excitation wavelength (Figure S50).

The optical response of the DQM-ALP nanoprobe to ALP was measured in a solution of Tris-buffer solution (TBS, 10 mM, pH 8.0, containing 1% DMSO). The fluorescence profile of DQM-ALP (10 μM) changed significantly as the ALP concentration increased from 0 to 90 mU mL^{-1} (Figure 1c) at 37°C due to the scission of the phosphate monoester bond. This converted DQM-ALP into DQM-OH intermediate, and AIE was recovered in aqueous media. These transformations were confirmed by variations in the

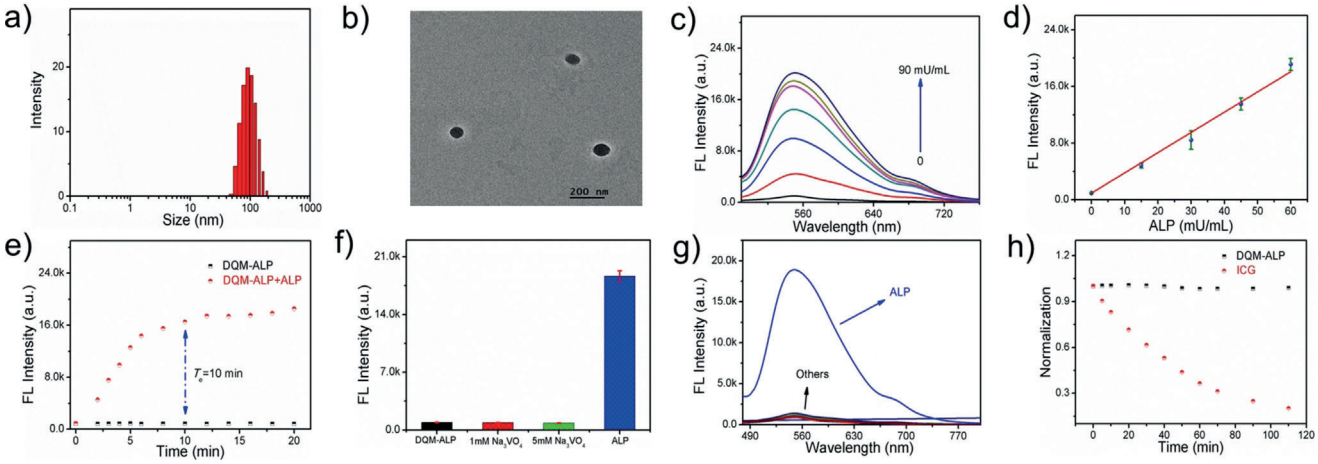

Figure 1. Morphology and spectral characterization of DQM-ALP probe. a) DLS characterization of DQM-ALP (10 μM) in the aqueous solution. b) TEM characterization of DQM-ALP (10 μM) in aqueous solution. c) Fluorescence spectra of DQM-ALP (10 μM) responding to ALP concentrations from 0 to 90 mU mL^{-1} at 37 °C. d) Linear fitting of the fluorescence intensity at 550 nm towards the low concentrations of ALP, incubation time 10 min. e) Response time of DQM-ALP (10 μM) in the absence (black) and presence (red) of ALP at 37 °C. f) ALP inhibition tests with Na_3VO_4 and DQM-ALP (10 μM) at 37 °C. g) Fluorescence spectra of DQM-ALP (10 μM) incubated with ALP and other analytes at 37 °C. The other analytes included Na^+ (100 μM), K^+ (100 μM), F^- (100 μM), Cl^- (100 μM), Br^- (100 μM), I^- (100 μM), NO_3^- (100 μM), CN^- (100 μM), S^{2-} (100 μM), HSO_4^- (100 μM), SCN^- (100 μM), ClO_4^- (100 μM), NO_2^- (100 μM), CH_3COO^- (100 μM), HCO_3^- (100 μM), CO_3^{2-} (100 μM), HPO_4^{2-} (100 μM), $H_2PO_4^-$ (100 μM), SO_4^{2-} (100 μM), ClO^- (100 μM), GSH (100 μM), Cys (100 μM), Hcy (100 μM), H_2O_2 (100 μM), ascorbic acid (100 μM), DTT (100 μM), β-galactosidase (β-Gal, 100 mU mL^{-1}), xanthine oxidase (XO, 100 mU mL^{-1}), acetylcholinesterase (AChE, 100 mU mL^{-1}), butyrylcholinesterase (BuChE), carboxylesterase (CE, 100 mU mL^{-1}), and alkaline phosphatase, (ALP, 75 mU mL^{-1}). h) Photostability of DQM-ALP (10 μM) and ICG dye (10 μM) under the same conditions. The experiments were repeated three times and the data were shown as mean (± S.D.).

absorption spectra (Figure S51), and characterization by DLS and TEM (Figures S52 and S53). Meanwhile, the color changes of probe solution indicated that DQM-ALP could be used to recognize ALP with the naked eye (Figure S54).

Activation by ALP converted DQM-ALP to tightly aggregated DQM-OH, indicating that the DQM-ALP nanoprobe formed loosely packed aggregates in the aqueous medium without fluorescence. The excellent linear relationship ($R^2 = 0.9942$) between the fluorescence intensity centered at 550 nm and various ALP concentrations (0–60 mU mL^{-1}) was obtained, as shown in Figure 1 d. Additionally, the detection limit of the DQM-ALP for ALP based on 3σ/slope formula was determined to be 0.15 mU mL^{-1}, which suggested that the sensitivity of DQM-ALP detection of ALP in vitro was high (Table S1). The Michaelis constant (K_m) and maximum initial reaction rate (V_{max}) were calculated to be 5.16 μM and 4.83 μM min^{-1} by Lineweaver–Burk analysis (Figure S55). Compared to without ALP group (Figure S56), the fluorescence intensity of DQM-ALP gradually increased to an equilibrium in the presence of ALP after 10 min (Figure 1 e and Figure S57), indicating that loose aggregation of amphiphilic structure of the DQM-ALP favored the ALP-mediated enzymatic reaction. When sodium orthovanadate (Na_3VO_4),[18] an ALP inhibitor was added to the solution, the fluorescence intensity of DQM-ALP was almost completely suppressed (Figure 1 f and Figure S58). To our satisfaction, only ALP induced a dramatic change in fluorescence behavior under identical conditions (Figure 1 g and Figure S59). This demonstrated that DQM-ALP could serve as an ALP-specific tool for monitoring ALP activity in complex biological samples. Photostability is another vital parameter used to evaluate the performance of fluorescent probes for biomedical applications, particularly the long-term monitoring of target activity for disease diagnosis and visual therapy. The commercial dye indocyanine green (ICG) has been approved for clinical use by the FDA.[19] Under irradiation with light at 350 mW cm^{-2} (Scheme S1), the absorbance spectra of commercial dye ICG distinctly decreased over time (Figure 1 h and Figure S60). In contrast, irradiation had no effect on the absorbance of DQM-ALP and DQM-OH (Figure 1 h and Figure S61 and S62), which clearly demonstrated that they could be used for long-term biological imaging. As illustrated in Figures S63 and S64, DQM-ALP showed good stability at pH values from 4.54 to 10.02 in aqueous solutions and optimum value of increased fluorescence intensity for the recognition of ALP at 37 °C. Our experimental results suggested that DQM-ALP would efficiently identify ALP activity under physiological conditions.

Docking Calculations and Verification of the Response Mechanism

To validate the relationship between DQM-ALP and ALP, docking calculations were performed using the Discovery Studio platform. We chose the crystal structure of ALP as the docking model.[20] As depicted in Figure 2 a,b, the DQM-ALP probe tended to approach the double zinc ion (named Zn_1^{2+} and Zn_2^{2+})[21] coordination center in the ALP cavity. The lengths of the coordinate bonds (Figure 2 c and Figure S65) between probe and ALP were 2.015 Å (O–Zn_1^{2+}), 2.041 Å (O–Zn_1^{2+}), and 2.829 Å (O–Zn_2^{2+}). These were extremely close to the inherent distances of the coordinate bonds between zinc ion and amino acid residues in ALP,

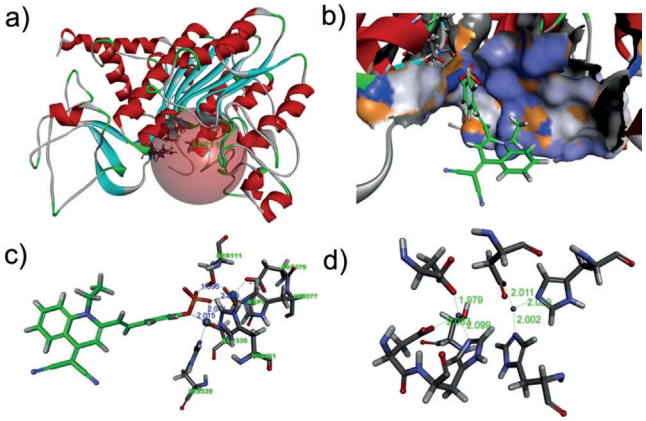

Figure 2. Docking of DQM-ALP on ALP based on Discovery Studio platform. a) Structure of ALP. The binding site is indicated by the red transparent sphere. b) Partial enlargement of (a). c) Lengths of coordinate bonds between DQM-ALP and ALP. d) Lengths of coordinate bonds between Zn^{2+} and amino acid residues in ALP.

which were 2.002 Å, 2.029 Å, 2.011 Å, 2.099 Å, 2.083 Å, and 1.979 Å (Figure 2d). With the help of the catalytic system centered on double zinc ion, the probe was transformed into the DQM-OH intermediate. This restored the AIE and strong fluorescence of the probe was measured, which was consistent with the process depicted in Scheme 1.

In addition, high resolution mass spectra were collected to confirm the generation of DQM-OH in vitro. A distinct peak at *m*/*z* 340.1449 was observed in the HRMS spectrum. This was in accordance with the calculated *m*/*z* of DQM-OH in positive mode, which was 340.1444 for $[M+H]^+$ (Figure S66), which further validated that DQM-OH resulted from ALP catalytic activity towards the DQM-ALP probe.

MTT Assays and Cell Imaging

Prior to cell fluorescence imaging, we examined the cytotoxicity of DCM-ALP and DQM-ALP using a standard MTT assay.[3f] As shown in Figures S67–S70, cell viability remained high after treatment with the probes for 24 h. The probes caused no noticeable cytotoxicity. Thus, the ability of DQM-ALP for imaging the activity of endogenous ALP was further investigated in living cells. Human cervical carcinoma cells (HeLa cells) and hepatoma carcinoma cells (HepG-2 cells) were chosen as model cells owing to their overexpression of ALP.[22] Compared to the control group (Figure 3b), obvious fluorescence signal (Figure 3e) was observed in HeLa cells incubated with DQM-ALP for 0.5 h. This was caused by in situ enzymatic dephosphorylation, which released the nanoaggregates DQM-OH. Similarly, this was also consistently observed in HepG-2 cells treated with DQM-ALP for 0.5 h (Figure S71). We also performed time-dependent imaging of DQM-ALP in live HeLa cells. As shown in Figure S72, fluorescence intensity increased sharply over 10 min, which was consistent with our in vitro characterization.

DQM-ALP inhibition experiments were performed to demonstrate that increased fluorescence intensity in living cells was triggered by ALP. When Na_3VO_4 were preincubated with HeLa cells for 1 h, followed by the addition of DQM-ALP for incubation another 0.5 h, the fluorescence intensity in the cells decreased (Figure 3h) until it eventually disappeared (Figure 3k), manifesting the activity of endogenous ALP inhibited by Na_3VO_4. Levamisole hydrochloride, another phosphatase inhibitor,[23] was less effective in inhibiting cellular ALP activity (Figure 3n,q). These results suggested that DQM-ALP probe could be activated by the overexpression of ALP in tumor cells for in situ monitoring of ALP activity, and that it could be employed for visual high-throughput screening ALP inhibitors. The advantages of two-photon fluorescence imaging include relatively low photo-

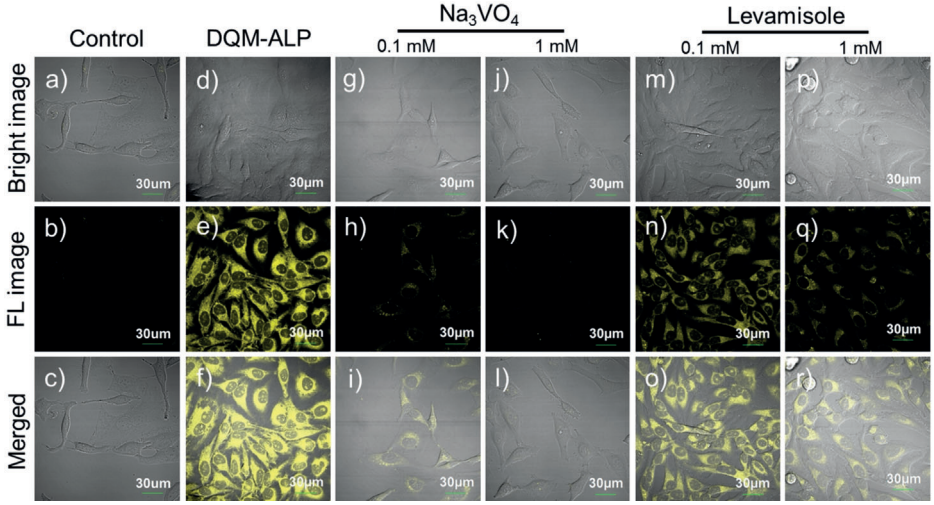

Figure 3. Confocal fluorescence images of HeLa cells incubated with DQM-ALP (10 μM) at 37°C. a–c) Control group, d–f) cells treated with DQM-ALP for 0.5 h; Na_3VO_4 group: Preincubated with g–i) 0.1 mM and j–l) 1 mM Na_3VO_4, followed by the addition of DQM-ALP for 0.5 h. Levamisole group: Preincubated with m–o) 0.1 mM and p–r) 1 mM levamisole, followed by the addition of DQM-ALP for 0.5 h. $\lambda_{ex}=473$ nm, $\lambda_{em}=490$–590 nm. Scale bar = 30 μm.

induced damage, photo-bleaching, deeper penetration, and higher spatial and temporal resolution. We thus evaluated the imaging performance of the probe using a two-photon platform. As expected, fluorescence was observed from HepG-2 cells treated with DQM-ALP under a Mai Tai femtosecond laser at 810 nm (Figure S73).

ALP plays a vital role in catalyzing the dephosphorylation of small molecules, proteins, and nucleic acids.[24] Thus, the visualization of ALP activity provides a simple and effective tool for chemical biology and clinical medicine. Previous studies have shown that sodium butyrate (NaBu) as an inducer increases the activity of ALP by stimulating de novo synthesis of the enzyme.[25] Therefore, HeLa cells were pre-incubated with NaBu to induce the synthesis of ALP mRNA.[26] After 4 h, there was no significant difference between the fluorescence intensities of the cells (Figure 4b) and the control group (Figure S74). Remarkable fluorescence was observed from the treated cells after 28 h and 48 h (Figure 4e,s), suggesting that ALP overactivity induced by NaBu had a time lag. As expected, the DQM-ALP was triggered by high ALP activity. Plenty of DQM-OH was generated, leading to the formation of aggregates in the cells and AIE fluorescence (Figure 4h). Cortisol was also used to increase the activity of HeLa ALP by modifying the enzyme during or shortly after synthesis, transforming the conformation of the enzyme protein, resulting in improved the catalytic efficiency.[27] Under 3 μM cortisol pretreatment, HeLa cells exhibited brighter yellow fluorescence (Figure 4n) than NaBu-stimulated cells after 28 h, in accordance with the pixel intensity of their channels (Figure 4s,t), which indicated that cortisol was a more efficient inducer than NaBu. These observations demonstrated that DQM-ALP could serve as an AIEgen probe with high spatiotemporal resolution (HSR) to monitor the upregulation of ALP activity.

Long-Term Cell Imaging Assessment

Long-term, high-fidelity bioimaging with AIEgens is of great importance in the field of biomedicine. We further investigated its ability to monitor the overexpression of ALP in cells with HSR over long periods of time. To demonstrate the inherent advantages of the AIE probe, the DCM-ALP (ACQ probe) based on the DCM-fluorophore modified with the same identification unit was used for the control group. Distinct fluorescence images (Figure 5b,n) were observed from the HeLa cells after incubation with DQM-ALP and DCM-ALP for 0.5 h, which indicated that both probes could be used to monitor ALP activity in the tumor cells. Fluorescence in the ACQ group (Figure 5q,z) nearly vanished within 3 h. However, the DQM-ALP group exhibited obvious intracellular fluorescence (Figure 5e), and the fluorescence intensity in the cells had only decreased to 66.98% of the original value (Figure 5y). These results suggested that DQM-ALP was activated by ALP to generate AIEgen aggregation in situ, which reduced the rate of exocytosis due to a size effect. The sharp drop in fluorescence in the control group was attributed to the ACQ effect and extracellular

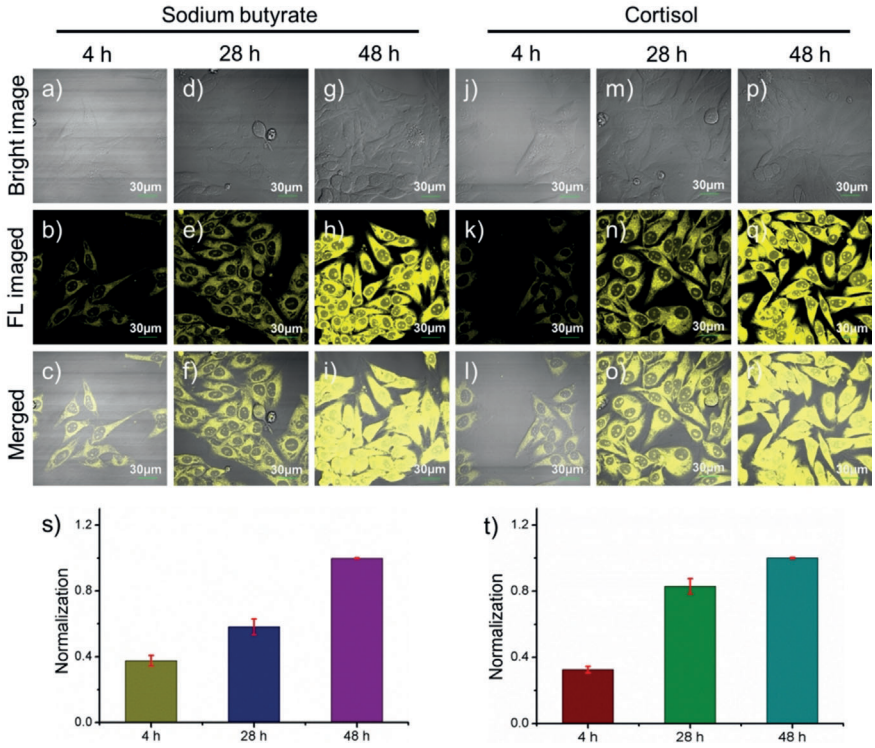

Figure 4. Confocal fluorescence images of endogenous ALP activity in the living HeLa cells induced by sodium butyrate (NaBu, 1 mM) and cortisol (3 μM) at 37 °C for 4 h (a–c and j–l), 28 h (d–f and m–o) and 48 h (g–i and p–r), followed by treatment with DQM-ALP for 0.5 h. s,t) The normalized fluorescence intensity of cells treated with sodium butyrate and cortisol, respectively. Note: the pixel intensity of each channel in images (h) and (q) was defined as 1.0. Error bar = RSD ($n = 9$), $\lambda_{ex} = 473$ nm, $\lambda_{em} = 490$–590 nm. Scale bar = 30 μm.

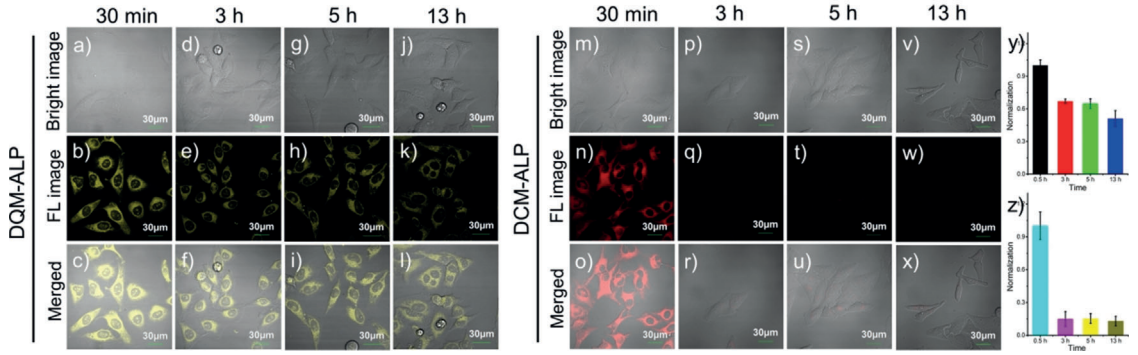

Figure 5. Long-term fluorescence imaging of HeLa cells treated with DQM-ALP. a–l) $\lambda_{ex}=473$ nm, $\lambda_{em}=490$–590 nm; m–x) $\lambda_{ex}=561$ nm, $\lambda_{em}=655$–755 nm. Normalized fluorescence intensities of cells incubated with DQM-ALP (y) and DCM-ALP (z). Note: The pixel intensity of each channel from the image (b) and (n) was defined as 1.0, respectively. Error bar = RSD ($n=9$). Scale bar = 30 μm.

leakage. Even after 13 h, the intracellular fluorescence intensity remained high level of 51.07 % of the original intensity (Figure 5 k,y).

Sub-organelle Localization Experiment

Co-localization experiments were carried out to further investigate the distribution of DQM-ALP in the cells after responding to ALP. HeLa cells were pre-treated with the DQM-ALP probe at 37 °C for 20 min. The commercial indicators (Hoechst 33342, LysoTracker Deep Red, and MitoTracker Deep Red FM) were then successively added into confocal dishes and incubated for another 20 min, respectively. As shown in Figure S75, the apparent fluorescence signal from the AIEgen nanoaggregates (Figure S75 f,j) overlapped well with the deep red fluorescence signal labeling by Lyso-Tracker (Figure S75 g) and Mito-Tracker dye (Figure S75 k) with high Pearson's correlation coefficients of 0.92 and 0.82. These were higher than that of the nucleus ($P=$ 0.32). These results demonstrated that the product of probe DQM-ALP responding to ALP mainly accumulated in lysosomes and mitochondria.

Multicellular Tumor Spheroid Imaging

3D-structured spheroids are used to better simulate the microenvironment of cells and reflects multicellular aggregation and avascular metastasis in vivo. Consequently, we evaluated the capability of enzyme-triggered DQM-ALP to be turned on inside cells of sub-millimeter 3D-structured spheroids. Exposure of the HeLa tumor spheroids to the DQM-ALP probe led to a significant increase in fluorescence under one-photon irradiation (Figure 6 a2–6 f2) accompanied by bright dots of aggregates, implying that the AIE probe was activated by the overexpression of ALP in the tumor spheroids. We also used DQM-ALP to monitor ALP activity in the HeLa spheroids on the two-photon microscope platform. Significant fluorescence enhancement was also observed (Figure 6 g2–6 l2), as time went on. Reconstructed 3D fluorescence images of HeLa spheroids treated with DQM-ALP were successfully obtained by scanning along the z-axis with two-photon excitation at 810 nm (Figure 6 m1–6 m3). With the advantage of two-photon longitudinal imaging, fluorescence was observed in each 8.48 μm layer of a HeLa tumor spheroid (Figure 6 C and Figure S76). Similar fluorescence was also observed in the HepG-2 tumor spheroids (Figures S77). This implied that ALP overexpression could activate more of DQM-ALP probes in the HepG-2 tumor spheroids in situ to generate the obvious AIE fluorescence signal. Our observations suggested that DQM-ALP was rapidly delivered into the 3D-structured spheroids and activated by ALP overexpression. This filled the gap between simple two-dimensional cell culture models and complex real tissues, resulting in a more vivid and economical research model for clinical and biological applications.

Imaging ALP Upregulation in a Drug-Induced Acute Liver Injury Model

The activation of DQW-ALP by ALP in vitro, in cells, and in tumor spheroids were assessed. The AIEgen probe was used to monitor the fluctuations in ALP activity in the drug-induced acute liver injury (DIALI) model. Overdoses of acetaminophen (APAP) can cause acute liver injury. This is generally accompanied by an increase in the ALP level. Compared to PBS-treated mice (Figure 7 b), the surfaces of livers in mice administered with APAP were covered with many hepatic parenchymal injury areas (Figure 7 g). The livers became lighter in color and nuclei of the tissue sections were wrinkled (Figure 7 h), which indicated the DIALI model was smoothly established. 20 μm sections of normal liver and DIALI liver tissue were prepared using a freezing microtome and incubated with the DQM-ALP probe. Isolated liver tissue from the mice pre-treated with APAP for 12 h, followed by incubation with DQM-ALP probe showed distinct AIE with increasing time (Figure 7 i and Figure S78). This indicated that the ALP content increased in the liver due to APAP-induced liver injury. In contrast, the fluorescence intensity in liver tissues from Balb/c mice pre-treated with PBS did not increase significantly after incubation with DQM-ALP (Figure 7 d and Figure S79). These results suggested that the

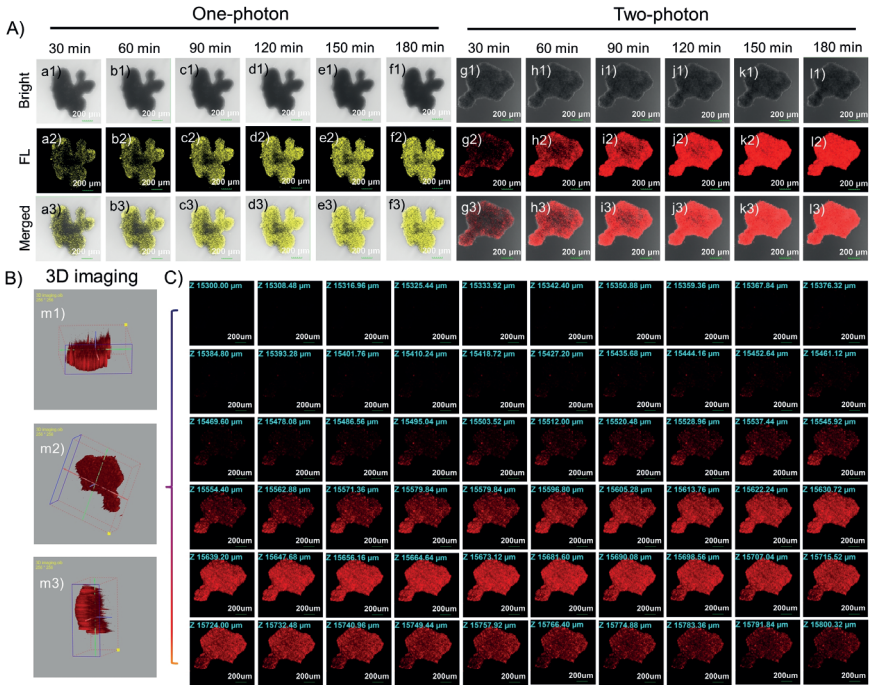

Figure 6. One- and two-photon microscope fluorescence imaging of HeLa multicellular tumor spheroids treated with DQM-ALP. A) One-photon model: a1–a3) 30 min; b1–b3) 60 min; c1–c3) 90 min; d1–d3) 120 min; e1–e3) 150 min; and f1–f3) 180 min. Two-photon model: g1–g3) 30 min; h1–h3) 60 min; i1–i3) 90 min; j1–j3) 120 min; k1–k3) 150 min; and l1–l3) 180 min. B) 3D tumor spheroid images (m1–m3) obtained along the *z*-axis direction at depths of 15 300–15 800 μm by each interval of 8.48 μm as a step (C). One-photon mode: λ_{ex} = 488 nm, λ_{em} = 520–620 nm; two-photon mode: λ_{ex} = 810 nm, λ_{em} = 575–630 nm. Scale bar = 200 μm.

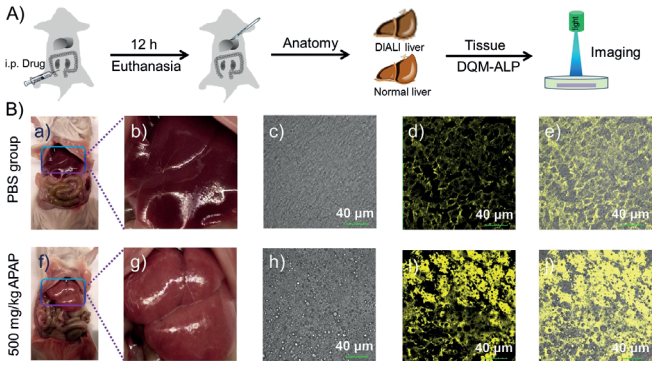

Figure 7. Imaging ALP up-regulation in the drug-induced acute liver injury model. A) Schematic illustration of APAP administered to Balb/c mice and fluorescence imaging of tissue sections. B) Mice treated with PBS (a–e) or APAP (500 mg kg^{-1}, f–j) for 12 h, followed by incubation with DQM-ALP (10 μM). λ_{ex} = 488 nm, λ_{em} = 520–620 nm. Scale bar = 40 μm.

probe could be used to monitor fluctuations in ALP activity induced by APAP in mouse liver, which was favorable for early DIALI predictions.

Differentiating Tumor Tissue from Normal Tissue

Accurate identification of tumor tissue and normal tissue is very important for the surgical resection of tumors to prevent recurrence, reduce cutting, and to avoid damaging normal tissue. We investigated whether the DQM-ALP probe could distinguish between tumor tissue and normal tissue. After the addition of probe DQM-ALP, hepatocellular carcinoma tissues exhibited the evident granular fluorescent spots just 10 min later (Figure 8 a2) owing to the generation of nanoaggregates due to ALP overexpression. The fluorescence intensity of DQM-ALP increased with prolonged incubation (Figure 8 a2–8 e2). No obvious fluorescence was observed in normal liver tissue (Figure 8 f2–8 j2), which suggested that the DQM-ALP probe could be used to differentiate between tumor tissue and normal tissue. In addition, cervical cancer tissues were also used to as a research model owing to overexpression of ALP. Strong fluorescence appeared in the tumor tissues (Figure 8l2 and Figure S80). Fluorescence in normal tissue was negligible (Figure 8 k2). Interestingly, 3D tissue imaging performed with two-photon platform, provided images that showed deep permeation of the probe into tissue and its activation by ALP overexpression in 100 μm hepatocellular carcinoma tissue (Figure 8 m1–8 m3 and Figures S81 and S82) and cervical cancer tissue (Figure 8 n1–8 n3) pre-loaded with DQM-ALP for 30 min. These results showed that the DQM-ALP could efficiently permeate tumor tissues and be selectively activated by ALP overexpression. Aggregation resulted in strong AIE fluorescence, which would allow tumors to be distinguished from normal tissue.

Visualization ALP Activity in Mice Xenograft Tumor Model

We then evaluated the performance of DQM-ALP for monitoring ALP activity in mice bearing tumor xenografts.

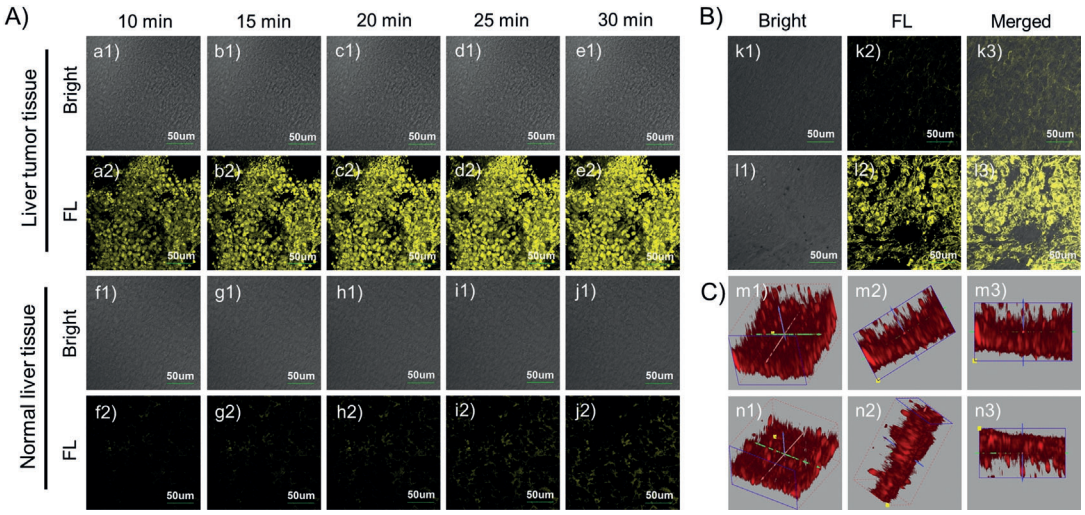

Figure 8. 2D and 3D imaging of tissues treated with DQM-ALP to monitor ALP activity. A) Time-dependent fluorescence imaging of 10 μm hepatocellular carcinoma tissue (a–e) and normal liver tissue (f–j). B) 2D fluorescence imaging of 10 μm normal tissue tissue (k1–k3) and cervical cancer tissue (l1–l3) were treated with DQM-ALP for 30 min. C) 3D fluorescence imaging of 100 μm hepatocellular carcinoma tissue (m1–m3) and cervical cancer tissue (n1–n3) under two-photon excitation. One-photon mode: $\lambda_{ex} = 488$ nm, $\lambda_{em} = 520–620$ nm; two-photon mode: $\lambda_{ex} = 810$ nm, $\lambda_{em} = 575–630$ nm. Scale bar = 50 μm.

Upon tumor formation, ex vivo imaging of the dissected organs and tumors after immersion in DQM-ALP was carried out using small-animal imaging equipment. As shown in Figure S83, HepG-2 tumor exhibited brighter fluorescence than other organs including the heart, liver, spleen, lung, and kidney after soaking for 15 min, which reached equilibrium in 1 h (Figure 9a). HeLa tumor also exhibited significant signal (Figure 9c) compared to normal liver (Figure 9b,d), which was caused by overexpression ALP in the tumor. A rapid fluorescence increase of the DQM-ALP-treated group was observed in the tumor region (Figure 9e–h) of tumor-bearing mice, demonstrating that DQM-ALP probe could rapidly monitor the ALP activity in mice. Fluorescence-guided surgery has attracted much attention in clinical research to achieve accurate resection of tumors. The biggest bottleneck for this technology is the lack of suitable clinical contrast agents, particularly activatable agents for high-fidelity imaging. We explored the use of probe for fluorescence-mediated surgical resection. As shown in Figure 9C, by direct spraying DQM-ALP probe in situ, fluorescence was remarkable in the cancerous tissue and there was a clear boundary between tumor tissue and normal tissue (Figure 9j). With fluorescence guidance, the tumor tissue was successfully removed intact using a scalpel (Figure 9k).

Conclusion

In summary, we rationally designed and synthesized the activatable AIEgen DQM-ALP for the specific monitoring of ALP activity. Owing to its matched amphiphilic structure, molecules DQM-ALP could form the loose nanoprobe by self-assembly in aqueous solution. Their formation was confirmed through the characterization of DLS and TEM. Detection of ALP activity with nanoprobe DQM-ALP was rapid and highly sensitive. The recognition of DQM-ALP by ALP was verified with docking calculations and HRMS analysis. DQM-ALP exhibited its inherent AIE fluorescence in response to ALP overexpression in tumor cells. The probe was firstly used to monitor the down-regulation of ALP activity with sodium orthovanadate and levamisole hydrochloride, and the up-regulation of ALP activity by sodium butyrate and cortisol stimulation. Unlike DCM-ALP, the DQM-ALP probe was visualized for up to 13 h in high-fidelity cell imaging. Under two-photon platform, DQM-ALP probe was delivered into 3D-structured spheroids to monitor spatially heterogenous ALP activity with high spatial resolution. Moreover, relying on abnormal ALP activity, DQM-ALP was successfully used to differentiate between tumors tissues and normal tissues in nude BABL/c mice bearing HepG-2 and HeLa xenograft tumors. Thus, we expect that the enzyme-activated AIEgen DQM-ALP can be a valuable tool for the early diagnosis and resection of cancerous tissues.

Acknowledgements

This work was supported by grants from the National Research Foundation of Korea (NRF) funded by the Korean government (MSIP) (No. 2012R1A3A2048814 for J. Y.), and National Science Foundation of China (No. U1608222 for X. P.). Mass spectral data were obtained from the Korea Basic Science Institute (Daegu) on a Jeol JMS 700 high-resolution mass spectrometer.

Conflict of interest

The authors declare no conflict of interest.

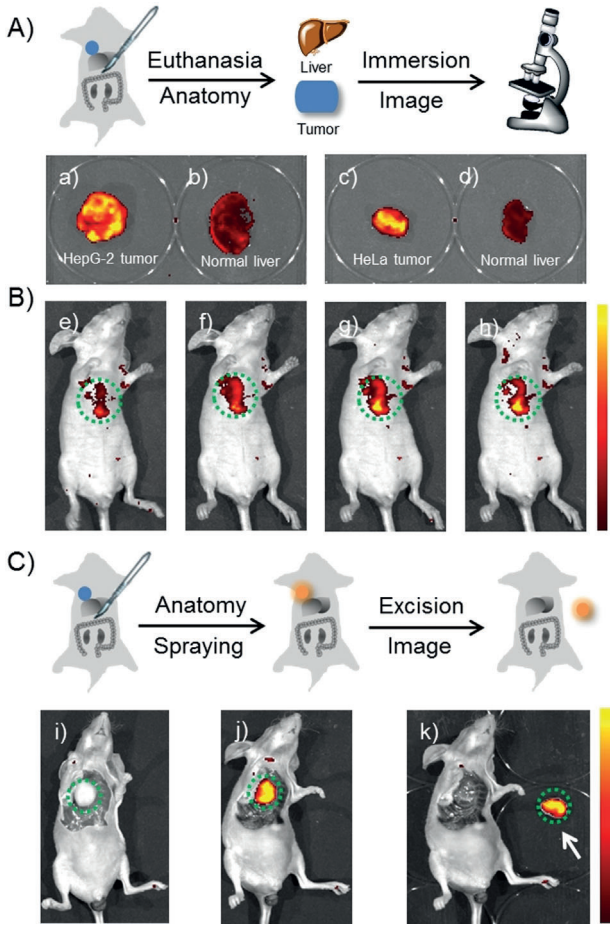

Figure 9. Fluorescence images of endogenous ALP activity in nude BABL/c mice bearing xenograft tumors. A) Schematic illustration of tumor and normal liver immersion in DQM-ALP solution (50 μM): a) HepG-2 tumor, b) normal liver, c) HeLa tumor, and d) normal liver. B) Fluorescence imaging of HeLa tumor-bearing Balb/c mice at various times (e, 0 min; f, 15 min; g, 30 min; h, 35 min) after injection with DQM-ALP, and the green areas represent the tumor. C) Schematic illustration of tumor resection by spraying DQM-ALP and fluorescence-mediated tumor resection: i) fluorescence image (control group), j) pre-treated by spraying DQM-ALP (50 μM), followed by fluorescence image, k) surgical removal of tumor, and the green areas represent the tumor. Fluorescence imaging of mice were recorded through small-animal imaging equipment (PerkinElmer IVIS Spectrum).

Keywords: aggregation-induced emission · AIEgens · enzyme activity · nanoprobes · tumor detection

[1] a) E. Ohuchi, K. Imai, Y. Fujii, H. Sato, M. Seiki, Y. Okada, *J. Biol. Chem.* **1997**, *272*, 2446–2451; b) M. Seiki, *Cancer Lett.* **2003**, *194*, 1–11.

[2] a) R. Pasqualini, E. Koivunen, R. Kain, J. Lahdenranta, M. Sakamoto, A. Stryhn, R. A. Ashmun, L. H. Shapiro, W. Arap, E. Ruoslahti, *Cancer Res.* **2000**, *60*, 722–727; b) H. Li, Y. Li, Q. Yao, J. Fan, W. Sun, S. Long, K. Shao, J. Du, J. Wang, X. Peng, *Chem. Sci.* **2019**, *10*, 1619–1625.

[3] a) A. Pompella, V. De Tata, A. Paolicchi, F. Zunino, *Biochem. Pharmacol.* **2006**, *71*, 231–238; b) T. Nishihara, H. A. Yoshihara, H. Nonaka, Y. Takakusagi, F. Hyodo, K. Ichikawa, E. Can, J. A. Bastiaansen, Y. Takado, A. Comment, *Angew. Chem. Int. Ed.* **2016**, *55*, 10626–10629; *Angew. Chem.* **2016**, *128*, 10784–10787; c) F. Wang, Y. Zhu, L. Zhou, L. Pan, Z. Cui, Q. Fei, S. Luo, D. Pan, Q. Huang, R. Wang, C. Zhao, H. Tian, C. Fan, *Angew. Chem. Int. Ed.* **2015**, *54*, 7349–7353; *Angew. Chem.* **2015**, *127*, 7457–7461; d) Y. Park, Y.-M. Ryu, T. Wang, Y. Jung, S. Kim, S. Hwang, J. Park, D.-J. Bae, J. Kim, H. Moon, H.-S. Lim, S.-Y. Kim, E. Chung, K. H. Kim, S. Kim, S.-J. Myung, *Adv. Funct. Mater.* **2018**, *28*, 1703450; e) Y. Urano, M. Sakabe, N. Kosaka, M. Ogawa, M. Mitsunaga, D. Asanuma, M. Kamiya, M. R. Young, T. Nagano, P. L. Choyke, H. Kobayashi, *Sci. Transl. Med.* **2011**, *3*, 110ra119; f) H. Li, Q. Yao, F. Xu, N. Xu, R. Duan, S. Long, J. Fan, J. Du, J. Wang, X. Peng, *Biomaterials* **2018**, *179*, 1–14.

[4] a) M. Tsujii, S. Kawano, R. N. DuBois, *Proc. Natl. Acad. Sci. USA* **1997**, *94*, 3336–3340; b) A. Goel, C. R. Boland, D. P. Chauhan, *Cancer Lett.* **2001**, *172*, 111–118; c) H. Zhang, J. Fan, J. Wang, B. Dou, F. Zhou, J. Cao, J. Qu, Z. Cao, W. Zhao, X. Peng, *J. Am. Chem. Soc.* **2013**, *135*, 17469–17475; d) A. K. Yadav, C. J. Reinhardt, A. S. Arango, H. C. Huff, L. Dong, M. G. Malkowski, A. Das, E. Tajkhorshid, J. Chan, *Angew. Chem. Int. Ed.* **2020**, *59*, 3307–3314.

[5] a) P. H. Lange, J. L. Millan, T. Stigbrand, R. L. Vessella, E. Ruoslahti, W. H. Fishman, *Cancer Res.* **1982**, *42*, 3244–3247; b) I. McDicken, G. Stamp, P. McLaughlin, P. Johnson, *Int. J. Cancer* **1983**, *32*, 205–209; c) H. W. Liu, K. Li, X. X. Hu, L. Zhu, Q. Rong, Y. Liu, X. B. Zhang, J. Hasserodt, F. L. Qu, W. Tan, *Angew. Chem. Int. Ed.* **2017**, *56*, 11788–11792; *Angew. Chem.* **2017**, *129*, 11950–11954; d) J. Liang, R. T. K. Kwok, H. Shi, B. Z. Tang, B. Liu, *ACS Appl. Mater. Interfaces* **2013**, *5*, 8784–8789.

[6] a) X. Wang, P. Li, Q. Ding, C. Wu, W. Zhang, B. Tang, *J. Am. Chem. Soc.* **2019**, *141*, 2061–2068; b) W. Fu, C. Yan, Z. Guo, J. Zhang, H. Zhang, H. Tian, W.-H. Zhu, *J. Am. Chem. Soc.* **2019**, *141*, 3171–3177; c) Z. Chen, X. Mu, Z. Han, S. Yang, C. Zhang, Z. Guo, Y. Bai, W. He, *J. Am. Chem. Soc.* **2019**, *141*, 17973–17977; d) D. Cheng, Y. Pan, L. Wang, Z. Zeng, L. Yuan, X. Zhang, Y.-T. Chang, *J. Am. Chem. Soc.* **2017**, *139*, 285–292; e) Q. Miao, D. C. Yeo, C. Wiraja, J. Zhang, X. Ning, C. Xu, K. Pu, *Angew. Chem. Int. Ed.* **2018**, *57*, 1256–1260; *Angew. Chem.* **2018**, *130*, 1270–1274; f) T. F. Brewer, G. Burgos-Barragan, N. Wit, K. J. Patel, C. J. Chang, *Chem. Sci.* **2017**, *8*, 4073–4081; g) Y. L. Pak, S. J. Park, D. Wu, B. Cheon, H. M. Kim, J. Bouffard, J. Yoon, *Angew. Chem. Int. Ed.* **2018**, *57*, 1567–1571; *Angew. Chem.* **2018**, *130*, 1583–1587; h) Q. Xu, C. H. Heo, G. Kim, H. W. Lee, H. M. Kim, J. Yoon, *Angew. Chem. Int. Ed.* **2015**, *54*, 4890–4894; *Angew. Chem.* **2015**, *127*, 4972–4976.

[7] a) X. Zhou, Y. Liu, Q. Liu, L. Yan, M. Xue, W. Yuan, M. Shi, W. Feng, C. Xu, F. Li, *Theranostics* **2019**, *9*, 4597–4607; b) G. Xu, Q. Yan, X. Lv, Y. Zhu, K. Xin, B. Shi, R. Wang, J. Chen, W. Gao, P. Shi, C. Fan, C. Zhao, H. Tian, *Angew. Chem. Int. Ed.* **2018**, *57*, 3626–3630; *Angew. Chem.* **2018**, *130*, 3688–3692; c) R. Yan, Y. Hu, F. Liu, S. Wei, D. Fang, A. J. Shuhendler, H. Liu, H.-Y. Chen, D. Ye, *J. Am. Chem. Soc.* **2019**, *141*, 10331–10341; d) E.-J. Kim, R. Kumar, A. Sharma, B. Yoon, H. M. Kim, H. Lee, K. S. Hong, J. S. Kim, *Biomaterials* **2017**, *122*, 83–90; e) H.-B. Cheng, Y.-M. Zhang, Y. Liu, J. Yoon, *Chem* **2019**, *5*, 553–574; f) X. Li, C.-y. Kim, S. Lee, D. Lee, H.-M. Chung, G. Kim, S.-H. Heo, C. Kim, K. S. Hong, J. Yoon, *J. Am. Chem. Soc.* **2017**, *139*, 10880–10886; g) X. Li, S. Yu, Y. Lee, T. Guo, N. Kwon, D. Lee, S. C. Yeom, Y. Cho, G. Kim, J.-D. Huang, S. Choi, K. T. Nam, J. Yoon, *J. Am. Chem. Soc.* **2019**, *141*, 1366–1372.

[8] a) D. Wang, B. Z. Tang, *Acc. Chem. Res.* **2019**, *52*, 2559–2570; b) K. Gu, W. Qiu, Z. Guo, C. Yan, S. Zhu, D. Yao, P. Shi, H. Tian, W.-H. Zhu, *Chem. Sci.* **2019**, *10*, 398–405; c) J. Mei, N. L. Leung, R. T. Kwok, J. W. Lam, B. Z. Tang, *Chem. Rev.* **2015**, *115*, 11718–11940.

[9] J. Luo, Z. Xie, J. W. Lam, L. Cheng, H. Chen, C. Qiu, H. S. Kwok, X. Zhan, Y. Liu, D. Zhu, B. Z. Tang, *Chem. Commun.* **2011**, *47*, 1740 – 1741.
[10] a) C. Xu, H. Zou, Z. Zhao, P. Zhang, R. T. Kwok, J. W. Lam, H. H. Sung, I. D. Williams, B. Z. Tang, *Adv. Funct. Mater.* **2019**, *29*, 1903278; b) S. Xu, Y. Duan, B. Liu, *Adv. Mater.* **2020**, *32*, 1903530; c) G. Qi, F. Hu, Kenry, D. Mao, S. Zhou, M. Wu, W. Wu, B. Liu, *Angew. Chem. Int. Ed.* **2019**, *58*, 16229 – 16235; *Angew. Chem.* **2019**, *131*, 16375 – 16381; d) M. Kang, C. Zhou, S. Wu, B. Yu, Z. Zhang, N. Song, M. M. S. Lee, W. Xu, F.-J. Xu, D. Wang, *J. Am. Chem. Soc.* **2019**, *141*, 16781 – 16789; e) Z. Zheng, D. Li, Z. Liu, H. Q. Peng, H. H. Sung, R. T. Kwok, I. D. Williams, J. W. Lam, J. Qian, B. Z. Tang, *Adv. Mater.* **2019**, *31*, 1904799.
[11] a) R. T. K. Kwok, C. W. T. Leung, J. W. Y. Lam, B. Z. Tang, *Chem. Soc. Rev.* **2015**, *44*, 4228 – 4238; b) J. Mei, Y. Hong, J. W. Lam, A. Qin, Y. Tang, B. Z. Tang, *Adv. Mater.* **2014**, *26*, 5429 – 5479; c) Y. Yuan, S. Xu, X. Cheng, X. Cai, B. Liu, *Angew. Chem. Int. Ed.* **2016**, *55*, 6457 – 6461; *Angew. Chem.* **2016**, *128*, 6567 – 6571; d) Y. Hong, J. W. Lam, B. Z. Tang, *Chem. Soc. Rev.* **2011**, *40*, 5361 – 5388; e) H.-B. Cheng, Y. Li, B. Z. Tang, J. Yoon, *Chem. Soc. Rev.* **2020**, *49*, 21 – 31.
[12] Z. Guo, C. Yan, W. Zhu, *Angew. Chem. Int. Ed.* **2019**, https://doi.org/10.1002/anie.201913249; *Angew. Chem.* **2019**, https://doi.org/10.1002/ange.201913249.
[13] a) J. M. Squirrell, D. L. Wokosin, J. G. White, B. D. Bavister, *Nat. Biotechnol.* **1999**, *17*, 763 – 767; b) H. M. Kim, B. R. Cho, *Chem. Rev.* **2015**, *115*, 5014 – 5055; c) H. Li, Q. Yao, J. Fan, J. Du, J. Wang, X. Peng, *Biosens. Bioelectron.* **2017**, *94*, 536 – 543.
[14] E. C. Costa, A. F. Moreira, D. de Melo-Diogo, V. M. Gaspar, M. P. Carvalho, I. J. Correia, *Biotechnol. Adv.* **2016**, *34*, 1427 – 1441.
[15] a) A. Shao, Z. Guo, S. Zhu, S. Zhu, P. Shi, H. Tian, W. Zhu, *Chem. Sci.* **2014**, *5*, 1383 – 1389; b) A. Shao, Y. Xie, S. Zhu, Z. Guo, S. Zhu, J. Guo, P. Shi, T. D. James, H. Tian, W. H. Zhu, *Angew. Chem. Int. Ed.* **2015**, *54*, 7275 – 7280; *Angew. Chem.* **2015**, *127*, 7383 – 7388.
[16] B. L. Vallee, D. S. Auld, *Proc. Natl. Acad. Sci. USA* **1993**, *90*, 2715 – 2718.
[17] a) A. M. Shamsuddin, *Anticancer Res.* **1999**, *19*, 3733 – 3736; b) Y. Tan, L. Zhang, K. H. Man, R. Peltier, G. Chen, H. Zhang, L. Zhou, F. Wang, D. Ho, S. Q. Yao, Y. Hu, H. Sun, *ACS Appl. Mater. Interfaces* **2017**, *9*, 6796 – 6803; c) Y. Wu, S. Huang, J. Wang, L. Sun, F. Zeng, S. Wu, *Nat. Commun.* **2018**, *9*, 3983.
[18] N. Takahara, F. Herz, R. M. Singer, A. Hirano, L. G. Koss, *Cancer Res.* **1982**, *42*, 563 – 568.
[19] L. Cheng, C. Wang, L. Feng, K. Yang, Z. Liu, *Chem. Rev.* **2014**, *114*, 10869 – 10939.
[20] K. Ghosh, D. M. Tagore, R. Anumula, B. Lakshmaiah, P. Kumar, S. Singaram, T. Matan, S. Kallipatti, S. Selvam, P. Krishnamurthy, *J. Struct. Biol.* **2013**, *184*, 182 – 192.
[21] F. Sunden, I. AlSadhan, A. Lyubimov, T. Doukov, J. Swan, D. Herschlag, *J. Biol. Chem.* **2017**, *292*, 20960 – 20974.
[22] a) H. Zhang, P. Xiao, Y. T. Wong, W. Shen, M. Chhabra, R. Peltier, Y. Jiang, Y. He, J. He, Y. Tan, Y. Xie, D. Ho, Y.-W. Lam, J. Sun, H. Sun, *Biomaterials* **2017**, *140*, 220 – 229; b) Z. Gao, J. Sun, M. Gao, F. Yu, L. Chen, Q. Chen, *Sens. Actuators B* **2018**, *265*, 565 – 574.
[23] A. T. Ali, C. B. Penny, J. E. Paiker, C. van Niekerk, A. Smit, W. F. Ferris, N. J. Crowther, *Clin. Chim. Acta* **2005**, *354*, 101 – 109.
[24] T. Balbaied, E. Moore, *Biosensors* **2019**, *9*, 102.
[25] A. Morita, D. Tsao, Y. S. Kim, *Cancer Res.* **1982**, *42*, 4540 – 4545.
[26] F. Ito, J. Chou, *J. Biol. Chem.* **1984**, *259*, 2526 – 2530.
[27] M. Griffin, G. Price, K. Bazzell, R. Cox, N. Ghosh, *Arch. Biochem. Biophys.* **1974**, *164*, 619 – 623.

Manuscript received: February 1, 2020
Version of record online: ■■ ■■, ■■■■

Research Articles

Fluorescent Probes

H. Li, Q. Yao, F. Xu, Y. Li, D. Kim, J. Chung, G. Baek, X. Wu, P. F. Hillman, E. Y. Lee, H. Ge, J. Fan, J. Wang, S.-J. Nam, X. Peng,* J. Yoon* _____ ■■■■–■■■■

An Activatable AIEgen Probe for High-Fidelity Monitoring of Overexpressed Tumor Enzyme Activity and Its Application to Surgical Tumor Excision

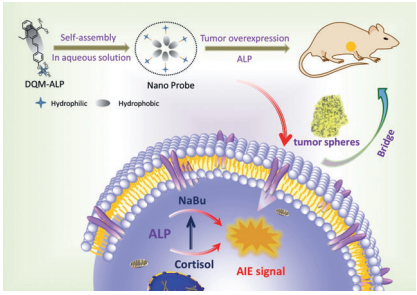

The cutting edge: An enzyme-activated two-photon AIEgen, DQM-ALP, for imaging the alkaline phosphatase (ALP) activity in tumor cells and 3D tumor spheroids with high spatial resolution was synthesized. DQM-ALP enabled accurate differentiation between tumor and normal tissue ex vivo and in vivo, suggesting that the probe may serve as a powerful tool to assist surgeons during tumor resection.